Title

Endogenous 1-deoxysphingolipid synthesis compromises anchorage-independent growth and plasma membrane endocytosis in cancer cells

Authors:

Thekla Cordes[1,2]

Ramya S. Kuna[1,2]

Grace H. McGregor[1,2]

Sanika V. Khare[1,2]

Jivani Gengatharan[1,2]

Thangaselvam Muthusamy[1]

Christian M. Metallo[1,2,*]

Affiliations:

[1]Department of Bioengineering, University of California, San Diego, La Jolla, CA 92093, USA

[2]Molecular and Cell Biology Laboratory, Salk Institute for Biological Studies, La Jolla, CA 92037, USA

*To whom correspondence should be addressed: Christian M. Metallo

E-mail: metallo@salk.edu

Short title:

Metabolic consequences of 1-deoxysphingolipids biosynthesis

Funding sources: This study was supported, in part, by US National Institutes of Health (NIH) grants R01CA234245 (C.M.M.) and R50CA252146 (T.C.).

Abbreviations:

[U-$^{13}C_{16}$]palmitate	Uniformly labeled palmitate containing 16 isotopic labeled carbons
Cer	Ceramides
CERS	Ceramide synthases
DEGS	Dihydroceramide desaturases
deoxyCer	Deoxy-ceramides
deoxyDHCer	Deoxy-dihydroceramides
deoxySA	1-deoxy-sphinganine
deoxySL	1-deoxysphingolipid
DHCer	Dihydroceramides
ER	Endoplasmic reticulum
FADS3	Fatty acid desaturase 3
FuB1	Fumonisin B1
HSAN1	Hereditary sensory neuropathy type I
Myr	Myriocin
SL	Sphingolipid
SPT	Serine palmitoyltransferase
SPTLC1^{C133W}	Mutant C133W serine palmitoyltransferase subunit LC1
SPTLC1^{WT}	Wildtype serine palmitoyltransferase subunit LC1

ABSTRACT

Serine palmitoyltransferase (SPT) predominantly incorporates serine and fatty acyl-CoAs into diverse sphingolipids that serve as structural components of membranes and signaling molecules within or amongst cells. However, SPT also uses alanine as a substrate in the contexts of low serine availability, alanine accumulation, or disease-causing mutations in hereditary sensory neuropathy type I (HSAN1), resulting in the synthesis and accumulation of 1-deoxysphingolipids. These species promote cytotoxicity in neurons and impact diverse cellular phenotypes, including suppression of anchorage-independent cancer cell growth. While altered serine and alanine can promote 1-deoxysphingolipid synthesis, they impact numerous other metabolic pathways important for cancer cells. Here we combined isotope tracing, quantitative metabolomics, and functional studies to better understand the mechanistic drivers of 1-deoxysphingolipid toxicity in cancer cells. Both alanine treatment and *SPTLC1*^{C133W} expression induce 1-deoxy(dihydro)ceramide synthesis and accumulation but fail to broadly impact the metabolism or growth of adherent cells. However, spheroid culture and soft agar colony formation were compromised when endogenous 1-deoxysphingolipid synthesis was induced. Consistent with these impacts on anchorage-independent cell growth, we observed that 1-deoxysphingolipid synthesis reduced plasma membrane endocytosis. These results highlight a potential role for SPT promiscuity in linking altered amino acid metabolism to plasma membrane endocytosis.

Keywords

Metabolism, soft agar, 1-deoxysphingolipids, RAB5, endocytosis, mitochondrial stress, alanine, serine, SPT promiscuity, plasma membrane

INTRODUCTION

Sphingolipids (SLs) are bioactive molecules and structural components of the cell membrane influencing essential cellular processes (1). Serine palmitoyltransferase (SPT) catalyzes the condensation of palmitate and serine in *de novo* biosynthesis of SLs but can also produce non-canonical, cytotoxic 1-deoxysphingolipids (deoxySLs) when using alanine or glycine as a substrate (2–4). Alterations in serine and alanine levels impact substrate availability for the promiscuous SPT reaction driving the accumulation of non-canonical SLs (5,6). DeoxySLs differ from canonical SL in that they lack the C_1-hydroxyl group of sphinganine, preventing further modification or degradation via canonical SL pathways (3). DeoxySLs are cytotoxic to cells, though specific mechanisms remain unclear (7–9). Accumulation of deoxySLs in the contexts of extracellular matrix detachment and/or serine deprivation compromises anchorage-independent growth and the establishment of xenograft tumors (10). However, serine and glycine restriction impact numerous downstream pathways, including nucleotide synthesis/one carbon metabolism (11–14), NAD(P)H (15–17), and lipid metabolism (10,18). On the other hand, exogenous addition of deoxySLs impacts various cellular processes, including mitochondrial function (8), autophagy (19), migration (20), sphingosine kinase 1 proteolysis (21,22), and protein folding (23), but this approach does not recapitulate the location and trafficking of deoxySLs actively synthesized on the endoplasmic reticulum (ER). We therefore aimed to determine deoxySL specific toxic effects independent of the broader metabolic impacts of serine and glycine restriction.

Alanine is abundant in the plasma and accumulates in diseases associated with mitochondrial dysfunction (24), metabolic syndrome (25,26), or anoxia (23). Transaminases expressed in cancer cells readily metabolize alanine and alpha-ketoglutarate to pyruvate and glutamate, but a reduction in pyruvate oxidation will cause alanine accumulation and subsequent conversion to deoxySA (10). Alanine supplementation therefore offers a means of driving deoxySL accumulation without restricting serine. Further, deoxySLs accumulate in the context of point mutations in *SPTLC1* or *SPTLC2* that occur in patients with hereditary sensory neuropathy type I (HSAN1), which increase the complex's affinity for alanine (2,4,27). Ectopic

expression of such *SPTLC1* variants effectively drives the endogenous accumulation of deoxySL in cells (27–30) offering an additional means of probing deoxySL-specific cellular effects.

Here we investigate how deoxySL biosynthesis alters membrane lipid metabolism and cellular processes, comparing 2D cell growth to anchorage-independent conditions. By combining high-resolution mass spectrometry, fluorescence imaging, and anchorage-independent growth studies, we highlight key aspects of deoxySLs on cancer cell metabolism and growth. These results demonstrate the impact of deoxySL on soft agar colony growth and endocytosis at the plasma membrane, illustrating key functional impacts relevant for cancer and neuropathy.

RESULTS

Alanine promotes deoxySL synthesis and compromises early spheroid formation

To better understand how cytotoxic deoxySLs impact cell function, we altered alanine availability to drive endogenous deoxySL biosynthesis in 2D cultures. Alanine is highly synthesized in proliferating mammalian cells cultured *in vitro* but absent from most media. Supplementation of 0.5 - 1 mM alanine increased deoxy-dihydroceramides (deoxyDHCer) and deoxy-ceramides (deoxyCer) pools by ~50%. At the same time, levels of canonical dihydroceramides (DHCer) and ceramides (Cer) were not significantly affected (Fig. 1A). We also observed that UK5099, an inhibitor of the mitochondrial pyruvate carrier (MPC), decreased alanine levels by promoting its oxidation (Fig. 1B, S1A). In turn, modulation of MPC and alanine levels had a strong impact on free deoxySA m18:0 in HCT116 cells (Fig. 1C). Further, numerous deoxyDHCer and deoxyCer species increased in response to alanine while UK5099 buffered their accumulation (Fig. 1D, S1B). These data highlight the direct impact of alanine and MPC function on deoxySL accumulation. Notably, exogenous alanine did not impact cell growth in 2D adherent culture, despite increasing non-canonical deoxySL species (Fig. 1E). We recapitulated our findings using A549 non-small lung cancer cells, further indicating that different cell types can accumulate deoxySL without exhibiting cytotoxicity (Fig. S1C, D).

In contrast to adherent culture models, we have previously demonstrated that alanine supplementation and deoxySL accumulation specifically compromises spheroid growth (10). Spheroid growth requires cells to initially survive upon trypsinization and sub-culture into anchorage-independent conditions; this process has a profound influence on glycans and downstream metabolic processes important for rebuilding these membrane structures (31). Subsequently, cells in spheroid culture must sustain proliferation in larger 3D structures which establish nutrient and hypoxic gradients and associated imbalances in redox pathways (32–34). To better understand how alanine and deoxySL metabolism impact spheroid growth we plated cells in low attachment plates and modulated deoxySL synthesis by supplementing alanine or inhibiting the MPC (UK5099), the SPT complex (myriocin), or ceramide synthases (CERS) (fumonisin B1). We added treatments at early (days 0-3) or late (days 3-8) spheroid formation phase and compared our results to spheroid treated continuously (days 0-8) as previously described (10) (Fig. 1F). Intriguingly, we observed an impact on spheroid biomass only when cells were treated in the early phase (i.e. Early and Continuous), while treatment during later stages of spheroid growth had no effect (Fig. 1G). Remarkably, these changes were recapitulated by all biochemical treatments, including alanine, UK5099, myriocin, and fumonsin B1. These data highlight that alanine and downstream deoxyDHCer and/or deoxyCer accumulation compromises growth during the early phase of spheroid formation rather than modulating growth/survival in larger spheroid structures.

Impact of endogenous deoxySL synthesis on metabolic fluxes

To elucidate the biochemical and functional impacts of endogenously synthesized deoxySLs independent of alanine supplementation, which can create NAD(H) or amino acid imbalances, or serine restriction, which can impact various downstream pathways, we established a doxycycline-inducible means of accumulating deoxySLs in cells. Indeed, ectopic expression of mutant SPTLC1 protein variants or fusion proteins robustly drives deoxySL accumulation in cultured cells (27–29). Here, we expressed doxycycline-inducible constructs containing either wild-type (grey: $SPTLC1^{WT}$) or mutant (red: $SPTLC1^{C113W}$) *SPT* in HCT116 cells via lentiviral delivery. $SPTLC1^{C113W}$ has an increased affinity for alanine, driving the

synthesis of deoxySLs compared to *SPTLC1*^{WT} (Fig. 2A) as observed in patients with HSAN1. We first confirmed that SPTLC1 protein variants were consistently expressed in cells (Fig. 2B). As expected, levels of deoxyDHCer and deoxyCer accumulated significantly in doxycycline-treated cells expressing *SPTLC1*^{C133W} compared to those infected with the *SPTLC1*^{WT} construct, while levels of DHCer and Cer were less affected (Fig. 2C). Further, all deoxySL species detected, including free deoxySA (Fig. S2A), deoxyDHCer (Fig. 2D), and deoxyCer (Fig. 2E), were robustly increased in *SPTLC1*^{C133W} compared to *SPTLC1*^{WT} expressing cells. On the other hand, levels of canonical DHCer and Cer species were less impacted in both polyclonal cell lines (Fig. S2B, S2C).

To further understand the turnover and metabolism of deoxySLs we next cultured cells in the presence of [U-$^{13}C_{16}$]palmitate and quantified ^{13}C incorporation into SL and deoxySL species using high-resolution mass spectrometry (Fig. 3A). Although this approach is limited by the non-physiological concentration and localization of the administered palmitate tracer, simultaneous quantitation of SL and deoxySL labeling kinetics is informative of the relative flux through each pathway. Notably, the more abundant SA, DHCer, and Cer pools rapidly achieved steady-state isotopic labeling and exhibited fast turnover (Fig. 3B, S3A). Labeling on both sphingoid bases and N-acyl chains was evident from M+32 isotopologues. While d18:0/16:0 DHCer pools achieved significant M+16 and M+32 labeling, SA and Cer only achieved intermediate levels of labeling, presumably due to contributions from lysosomal-derived sphingosine pool. On the other hand, deoxySA and deoxyDHCer were only detected in cells expressing *SPTLC1*^{C113W} and exhibited significantly lower labeling from [U-$^{13}C_{16}$]palmitate than canonical ceramides (Fig. 3C, S3B). Given the smaller pool sizes of deoxySLs and reduced labeling compared to canonical SLs (and slower labeling kinetics), these data indicate that *de novo* deoxySL synthesis and downstream turnover is much slower than that of canonical ceramides. Indeed, we failed to detect significant labeling in deoxyCer species (Fig. 3C), suggesting that conversion rates of this detoxification reaction (35) are relatively slow compared to (deoxy)SL biosynthesis. These results also support the concept that *SPTLC1*^{C113W} lacks the functional catalytic capacity of wild-type enzyme for production of canonical ceramides (Fig. 3B), which has been observed in iPSC-derived neuronal cultures (36).

To determine how deoxySL accumulation influenced other metabolic pathways we quantified broader labeling and flux changes occurring in *SPTLC1*^{WT} and *SPTLC1*^{C113W}-expressing cells. For example, palmitate oxidation and enrichment of citrate via acetyl-coenzyme A and citrate synthase were unaltered in both cell lines (Fig. 3D). Isotope enrichment from [U-$^{13}C_6$]glucose was similarly unchanged when deoxySL synthesis was active (Fig. S3C). In addition, doxycycline-treatment and deoxySL accumulation over 6 days failed to impact mitochondrial respiration measured by Seahorse (Fig. S3D). These results suggest that endogenous deoxySL synthesis is not sufficient to significantly alter central carbon metabolism or mitochondrial respiration. Indeed, adherent growth was not impacted by doxycycline-induced expression with increased deoxySL biosynthesis by expression of *SPTLC1*^{C133W}, suggesting that cells can accommodate a certain level of *de novo* synthesized deoxySLs (or canonical SLs) without experiencing deleterious effects on growth (Fig. 3E). Consistent with prior results (10) and those presented above (Fig. 1G), we observed a slight but significant reduction in spheroid growth in *SPTLC1*^{C133W} compared to *SPTLC1*^{WT} HCT116 cells suggesting that the stress from initiating non-adherent growth sensitizes cells to deoxySL accumulation induced toxicity (Fig. 3F).

We and others have also administered exogenous deoxySA to culture media for analysis of downstream effects (8,10,23), observing significant toxicity in some cell types. However, administration of free deoxySA significantly impacts its localization and thus local concentrations within cells compared to processing of newly synthesized deoxySLs on the ER membrane. In fact, we observed that deoxySA treatments, even at relatively moderate concentrations of 100 nM, resulted in a much greater accumulation of deoxyDHCer and deoxyCer species (~20 fold) compared to alanine supplementation or *SPTLC1*^{C133W} expression (2-5 fold) (Fig. 3G. S3E). These increases with deoxySA treatment were most pronounced in deoxyDHCer species containing very-long chain fatty acids (Fig. S3F) which are considered to be the most toxic (23). Notably, our adherent cell models achieved moderate, but more physiologically relevant, increases in deoxySL levels without showing overt cytotoxicity. Exogenous deoxySA administration may elicit distinct biological impacts due to aberrant localization of deoxySLs compared to that occurring via

synthesis on the ER membrane. Indeed, ceramide synthases are expressed in the mitochondria and can drive cellular toxicity (37–39).

Alanine and deoxySL synthesis influence colony formation in soft agar

Single-cell growth, migration, and invasive growth are hallmarks of transformed cells and correlate with anchorage-independent growth. As noted above, metabolically altering deoxySL synthesis consistently influenced "3D" anchorage-independent cell growth but not 2D adherent cell growth. To better understand the impact of deoxySL synthesis on proliferation in these contexts we next examined its impact on soft agar colony formation. Notably, we observed a significant growth defect in cells ectopically-expressing *SPTLC1*^{C133W} compared to *SPTLC1*^{WT} (Fig. 4A). We also rescued colony formation of *SPTLC1*^{C133W}-expressing cells using 10 nM myriocin, which had little impact on colony formation in cells expressing *SPTLC1*^{WT} (Fig. 4B). We also engineered the A549 non-small cell lung cancer cell line to express doxycycline-inducible *SPTLC1*^{WT} or *SPTLC1*^{C133W} (Fig. S4A). As in HCT116 cells, expression of *SPTLC1*^{C133W} potently increased deoxySLs (Fig. S4B) and suppressed soft agar colony formation in these cells (Fig. S4C). On the other hand, myriocin treatment blocked growth suppression induced by *SPTLC1*^{C133W} (Fig. S4C).

To further support these results, we next examined whether buffering deoxySA synthesis induced by alanine supplementation rescues colony formation. Addition of alanine to culture media consistently reduced soft agar growth of HCT116 cells, but targeted inhibition of SPT or MPC, which both prevent deoxySL accumulation, mitigated the negative effects of this supplementation (Fig. 4C). Similar trends in soft agar colony formation were observed when modulating deoxySL synthesis in A549 cells with alanine and myriocin (Fig. S4D). Intriguingly, normalizing the serine/alanine ratio by co-addition of serine to the culture medium also enhanced soft agar growth, providing an orthogonal biochemical means of rescuing these effects (Fig. 4D). Collectively, these results suggest that metabolically induced deoxySL accumulation specifically impacts soft agar growth, or more generally, cellular processes important for anchorage-independent growth.

DeoxySLs compromise plasma membrane endocytosis

The above studies demonstrate that deoxySL accumulation inhibits spheroid cell growth and soft agar colony formation. The temporal studies outlined in Figure 1F-G also highlighted the sensitivity of this process to cell seeding just after passaging, which induces membrane turnover facilitated by endocytosis. Soft agar growth also requires endocytic flux to catabolize matrix and establish multi-cellular colony formation. We therefore hypothesized that metabolic induction of deoxySL compromises plasma membrane endocytosis, which is mediated by GTPases such as RAB5. To directly examine whether this process was altered by deoxySL accumulation we quantified expression of the early endosomal marker RAB5, which regulates endosomal biogenesis and trafficking, in cells expressing $SPTLC1^{WT}$ or $SPTLC1^{C133W}$. RAB5 positive endosomes were significantly decreased in $SPTLC1^{C133W}$-expressing HCT116 cells compared to control conditions, indicating decreased endocytic activity (Fig. 5A). We also observed similar changes in A549 cells expressing $SPTLC1^{C133W}$ (Fig. 5B). Ectopic $SPTLC1^{C133W}$ expression induced reductions in RAB5 similar to that occurring with dynamin inhibition (Fig. 5A, B). Furthermore, we also observed decreased RAB5 positive endosomes in HCT116 cells induced to accumulate deoxySLs with alanine treatment, providing an additional link to defects in endocytosis (Fig. 5C). In fact, supplementation of both serine and alanine prevented this decrease in RAB5 positive endosomes from occurring (Fig. 5C). Collectively, these results demonstrate that genetic or metabolic alterations that promote deoxySL accumulation in cancer cells influence plasma membrane endocytosis, which manifests as defects in anchorage-independent growth.

DISCUSSION

Here we investigated the effects of endogenous deoxySL accumulation in cancer cells, using alanine supplementation or ectopic expression of $SPTLC1^{C133W}$. Our engineered cell systems allowed us to determine deoxySL-specific cellular effects independent of broader metabolic changes caused by serine and glycine deprivation. We observed that synthesis and accumulation of non-canonical deoxySLs

specifically compromised anchorage-independent growth without influencing central carbon metabolism or respiration. Rather, these amino acid-driven metabolic changes influence plasma membrane endocytosis, highlighting an important functional role for SPT promiscuity in coordinating such processes (Fig. 6). While deoxySA synthesis has negligible effects on adherent cancer cell growth, we observed reduced proliferation in soft agar colony assays, an environment which places significant load on the plasma membrane. Therefore, in the context of dietary serine/glycine restriction, elevated deoxySLs may compromise tumor seeding and combine with additional downstream metabolic effects to reduce tumor progression (40). On the other hand, deoxySL synthesis also influences T-cell function (41), which also must be considered in the context of cancer therapy. Collectively, these results clarify how deoxySL accumulation impacts cell metabolism and further highlight the impact of these species on membrane processes.

We also observed differences in cells that synthesized deoxySLs endogenously versus those treated with exogenous deoxySA. Notably, SPT, CERS, dihydroceramide desaturase (DEGS), and fatty acid desaturase 3 (FADS3) are predominantly localized to the ER membrane, catalyzing the synthesis and processing of (deoxy)DHCer and (deoxy)Cer species that are further trafficked to membranes throughout the cell. Therefore, proteins and organelles exposed to deoxySA via exogenous treatments versus endogenous synthesis will differ, which could account for lack of any pronounced effect observed with *SPTLC1*^{C133W} expression on intermediary metabolism. Diverse phenotypes have been proposed for cells and tissues exposed to deoxySA, including mitochondrial dysfunction and apoptosis (8,20). However, HSAN1 patients acquire specific sensory defects with age and do not present with broad metabolic dysfunction (42), suggesting the effects of deoxySL accumulation are more subtle or more specific to neurons. Rather, we observed specific effects of endogenously produced deoxySL on membrane processes that are critically important for anchorage-independent cancer cell growth and colony formation as well as neuronal function. As growth factor receptor-mediated signaling is intimately tied to plasma membrane trafficking, the impact on distinct signaling pathways warrants further investigation (43). Furthermore, deoxySA regulation of sphingosine kinase could impact signaling through S1P receptors (22). Karsai et al. also recently observed

that deoxySLs influence cell migration, which requires membrane dynamics for movement (20). Collectively these studies highlight key cellular phenotypes associated with deoxySL accumulation and membrane processes.

One key question that remains is the mechanism of toxicity for deoxySLs endogenously produced in the body (e.g. in patients with low serine). In our cell models we achieved a 2-5-fold increase of deoxySL levels in our cell models, similar to what is observed in Macular Telangiectasia (MacTel) patients with low serine (44). While deoxySL accumulation alone is not sufficient to drive macular defects (44), deoxySLs potentially combine with additional stresses (e.g. age, dyslipidemia) to drive pathogenesis via compromised membrane processing. More generally, by integrating metabolic signals from amino acid metabolism into the ER and plasma membrane, SPT promiscuity acts as an important conduit linking central carbon metabolism changes to the lipidome. This metabolic vulnerability may be exploited in certain tumor types through manipulation of amino acid metabolism (10) but may also contribute to neuropathy in patients (44). Here we have identified a key link between deoxySL accumulation and endocytosis in cancer cells, which is an important driver of tumor progression (45).

MATERIAL and METHODS

Reagents

Media and sera were purchased from Life Technologies. Isotope tracers were purchased from Cambridge Isotopes. Sphingolipid standards were purchased from Avanti polar lipids. All other reagents were purchased from Sigma unless otherwise noted.

Cells were treated at a concentration of 5 µM UK5099 (Cat. #PZ0160, Millipore Sigma), 10 nM myriocin (Myr, Cat. #M1177, Millipore Sigma), 10 µM fumonisin B1 (FuB1, Cat. #F1147, Millipore Sigma), or 20 µM Fenofibrate (Cat. #PHR1246, Sigma) with stock solutions prepared in DMSO. DeoxySA m18:0 (Cat. #860493P, Avanti), and amino acids were supplemented to growth media with concentrations as indicated in the text.

Cell culture

All cell lines were purchased from ATCC and tested negative for mycoplasma contamination: A549 (ATCC, CCL-185); HCT116 (ATCC, CCL-247); HEK293FT (ATTC, CRL-3216). Cells were cultured in Dulbecco's Modified Eagle Media (DMEM, Cat. #11965-092, Gibco) containing 25 mM glucose, 4 mM glutamine, 100 U/ml penicillin, and 100 µg/ml streptomycin in a humidified cell culture incubator at 37 °C and 5% CO_2. HCT116, A549, and HEK293T cells were cultured in growth medium containing 10% fetal bovine serum (FBS) (Cat. #16000-044, Gibco) and engineered *SPTLC1* expressing cell lines containing 10% tetracycline (TET)-free FBS (Cat. #FB15, Omega, Scientific. Inc.). Cells were detached with 0.05% trypsin-EDTA.

Engineering SPTLC1 expressing cell lines

SPTLC1 gene cDNA ORF nucleotide sequence (NM_006415) was purchased from GenScript. The ORF was subjected to point mutation to generate mutant $SPTLC1^{C133W}$ ORF and cloned into pCW57.1 vector (addgene Plasmid #41393). Briefly, the ORF and the plasmid were digested with Nhe1 and Age1, gel purified, and ligated. The engineered pCW57.1 plasmids containing $SPTLC1^{WT}$ or $SPTLC1^{C133W}$ were delivered into HCT116 and A549 cells using lentivirus delivery strategy.

Lentivirus were produced using HEK293T cells in high glucose DMEM supplemented with 10% FBS. One 10 cm cell culture dish of HEK293T cells at 60% confluency were transfected with 1.3 µg VSV.G/pMD2.G (addgene #12259), 5.3 µg lenti-gag/pol/pCMVR8.2 (addgene #12263), and 4 µg of the plasmid using 16 µL Lipofectamine 3000 diluted in 0.66 mL of OPTI-MEM (Life technology). Medium containing viral particles was harvested after 48 and 72 hours, filtered with 0.45 um filters, and further concentrated using Amicon Ultra15 centrifugal ultrafilters with a 100,000 NMWL cutoff (Cat. #UFC910024, Merck Millipore), and stored at -80°C until use.

Cells were infected in 6-well tissue culture plates with 6 µl concentrated virus particles in 0.5 ml growth medium containing 6 µg/ml polybrene for 4h before addition of 2 ml virus-free growth medium containing polybrene. After 24h, medium was changed to growth medium containing 2 µg/ml puromycin. After

puromycin selection, immunoblotting and RT-PCR analyses were carried out to confirm the expression of SPTLC1 in response to doxycycline as indicated in the text. For metabolic and functional experiments, HCT116 cells were induced with 0.1 µg/ml doxycycline and A549 cells with 1 µg/ml doxycycline.

Adherent cell growth assay using PrestoBlue

Cells were cultured in 96 well plates for 3 days with treatments as indicated in each figure. Cell viability was determined using PrestoBlue Cell viability Reagent (Invitrogen) per manufacturer's instructions.

Spheroid growth assay

For spheroid assays, 20,000 singularized cells were plated in 2 ml growth medium on 6-well ultra-low attachment plates (Cat. #3471, Corning) with treatments as indicated in the text (1 mM alanine, 5 µM UK5099, 10 nM myriocin, 20 µM fumonisin B1). HCT116 expressing cell lines were induced with 0.1 µg/ml doxycycline for 2 days prior seeding. Medium was changed on day 3 and 5. Growth was determined after 3-8 days as indicated in the text. Spheroids were collected in 2 ml sample tubes, centrifuged at 100 *g* for 5 min and the pellet was washed once with 2 ml 0.9% (w/v) NaCl. The spheroids were lysed with 100 µl RIPA buffer (Cat. #BP-115-5x, Boston Bioproducts) and homogenized with a ball mill (Retsch Mixer Mill MM400) at 30Hz for 3 min. The cell suspension was centrifuged at 20.000 *g* for 10 min at 4 °C and 20 µl of the supernatant was used for protein quantification using BCA protein assay kit (Cat. #G1002, Lamda Biotech. Inc) as per manufacturer's instruction.

Soft agar colony formation assay

Soft agar colony formation assay was conducted in 6-well tissue culture plates. A 3% low gelling temperature agarose (Cat. #A4018, Millipore Sigma) stock solution was prepared in water, autoclaved, and kept at 55 ºC in a water bath until use. 2 ml of the lower, hard layer containing of 0.6% in growth medium was added per well and allowed to solidify for 20 min at room temperature. 3000 cells were mixed with 1 ml of 0.3% agarose in growth medium supplemented with treatments of choice (DMSO, 5 µM UK5099,

10 nM myr, 1 mM serine, 0.5 mM or 1 mM alanine) as indicated in figure legends and overlayed on the lower, hard layer. The plates were placed at 4°C for 5 min to allow for a fast solidification improving uniform cell distribution in the soft agarose layer. The plates were then transferred into a humidified cell culture incubator at 37 °C with 5% CO_2 to allow colony formation. HCT116 colonies were counted on day 7 using a brightfield microscope.

Protein extraction and immunoblotting

Cells were plated on 6-well plates containing in growth medium containing 10% TET-free FBS and doxycycline for 4 days as indicated in the figure legend. Medium was changed on day 2. Cells were lysed in ice-cold RIPA buffer (Cat. #BP-115-5x, Boston Bioproducts) supplemented with 1x HALT protease inhibitor cocktail (Cat. #78430, Thermo Fisher Scientific), vortexed for 20 min at 4°C and centrifuged at 20.000 *g* for 10 min at 4 °C. Supernatant was used to quantify protein using BCA protein assay kit (Cat. #G1002, Lamda Biotech. Inc) and pre-diluted Protein Assay Standards (Cat. #23208, Thermo Scientific) as per manufacturer's instruction. Samples were incubated for 5 min at 95 °C in 4x laemmli buffer. 40 µg of total protein was separated on a 4–20% SDS-PAGE gel (mini-PROTEAN TGX gels, Bio-Rad) along with PageRuler Prestained protein ladder (Cat. #26619, Thermo Scientific) and proteins were transferred onto a PVDF membrane (Millipore, Cat. No. ISEQ00010). The membrane was blocked with 5% non-fat milk in tris buffered saline with 0.1% Tween 20 (TBS-T) for 1 h and immunoblotted with primary antibody at 4 °C overnight diluted in 5% non-fat milk. anti-SPTLC1 (1:1000 dilution, Cat. #15376-1-AP, Proteintech), anti-ß-actin (1:1000 dilution, Cat. #3700, Cell Signaling Technology). The immunoblots were then incubated with secondary antibody for 1 h at room temperature (1:1000 dilution, anti-rabbit Cat. #7074, lot 28, or anti-mouse HRP-conjugate Cat. #7076S, lot 32, Cell Signaling Technology). Specific signal was detected using SuperSignal West Pico Chemiluminescent Substrate (Cat. # 1705061, BioRad) and imaged with a BioRad ChemiDoc XRS+ imaging station. Band signal from Western Blots was determined using Image Lab Software from BioRad and normalized to signal of ß-actin. Antibodies for

western blotting were validated for human reactivity by the manufacturer and used per their instructions. Uncropped raw blots are provided in Extended Data 1.

Respirometry

Respiration was measured in adherent monolayers of cells using an Agilent Seahorse XFe96 Analyzer with a minimum of 5 cellular replicates per condition. Engineered *SPTLC1*^{C133W} expression cell line were cultured in the presence of doxycycline four days prior and two days after seeding on 96well plates in the presence of doxycycline. Cells were assayed in DMEM medium (Cat. #5030, Sigma Aldrich) supplemented with 8 mM glucose, 3 mM glutamine, 3 mM pyruvate, and 2 mM HEPES. Cells were washed twice with 100 µl assay medium and cultured in 150 µL assay medium for 1h before measurement. Respiration was measured under basal conditions as well as after injection of 2 µM oligomycin (Oligo) (Port A), sequential addition of 200 nM FCCP (Port C, D), and addition of 0.5 µM rotenone and 1 µM antimycin (Ant/Rot) (Port D). Oxygen consumption rates were normalized to protein content using BCA protein assay kit (Cat. #G1002, Lamda Biotech. Inc).

Isotopic tracing and analysis

Cells were cultured in medium containing stable isotope tracers of choice as indicated in the text. Tracers were purchased from Cambridge Isotopes Inc. or Sigma: [U-$^{13}C_6$]glucose (CLM-1396-25), [U-$^{13}C_{16}$]palmitate (CLM-409), and [2,3-$^{13}C_2$]alanine (Cat. #604682). For alanine tracing studies, HCT116 cells were cultured in growth medium supplemented with 1 mM ^{13}C alanine for 24h in the presence of DMSO or 5 µM UK5099. For glucose isotopic labeling experiments, HCT116 *SPTLC1* expressing cells were induced with 0.1 µg/ml doxycycline for 5 days before starting tracing for 24h. Tracing was performed with DMEM (Cat. #5030, Sigma Aldrich) medium where ^{12}C glucose replaced with 25 mM [U-$^{13}C_6$]glucose and 10% TET-free FBS was supplemented. Labeling on metabolites from ^{13}C alanine and ^{13}C glucose was quantified using GC-MS technology. Mass isotopomer distributions and total metabolite abundances were

computed by integrating mass fragments using a MATLAB based algorithm with corrections for natural isotope abundances as described previously (46,47).

For tracing studies with [U-$^{13}C_{16}$]palmitate, HCT116 cells were cultured in growth medium in the presence of 0.1 µg/ml doxycycline for 7 days before tracer start. Growth medium was replaced to DMEM medium containing 1% (v/v) delipidated FBS 24h prior tracer start and medium exchange again 1h prior tracer trace. [U-$^{13}C_{16}$]palmitate was noncovalently bound to fatty acid-free BSA and added to culture medium at 5% of the final volume (50 µM final concentration). Media was prewarmed to 37ºC in a cell incubator with 5% CO_2 and cells were traced for 15 min, 1 h, and 4 h. Metabolites were extracted, and labeling was quantified on a Q-Exactive LC-MS system. Metabolites were annotated and labeling was corrected for natural isotope abundance using Maven software v2011.6.17 (48). Due to [U-$^{13}C_{16}$]palmitate tracer purity of 98% (Cat#. #CLM-409, Cambridge Isotope Laboratories, Inc), we also observed a low fraction of labeled M+15 as well as M+31 on deoxyDHCer m18:0/16:0. In Figure S3B, M+16 depicts the combined label of M+15 and M+16, while M+32 depicts the combined label of M+31 and M+32.

Gas chromatograph - Mass spectrometry (GC-MS) and sample preparation

Metabolites were extracted, analyzed, and quantified, as previously described in detail (47). Briefly, cells were washed with saline solution and quenched with 0.25 ml -20 °C methanol. After adding 0.1 ml 4°C cold water, cells were collected in tubes containing 0.25 ml -20 °C chloroform. The extracts were vortexed for 10 min at 4 °C and centrifuged at 16,000 × *g* for 5 min at 4°C. The upper aqueous phase was evaporated under vacuum at 4 °C. Derivatization for polar metabolites was performed using a Gerstel MPS with 15 µl of 2% (w/v) methoxyamine hydrochloride (Thermo Scientific) in pyridine (incubated for 60 min at 45°C) and 15 µl N-tertbutyldimethylsilyl-N-methyltrifluoroacetamide (MTBSTFA) with 1% tert-butyldimethylchlorosilane (Regis Technologies) (incubated further for 30 min at 45 °C). Derivatives were analyzed by GC-MS using a DB-35MSUI column (30 m x 0.25 i.d. x 0.25 µm) installed in an Agilent 7890B gas chromatograph (GC) interfaced with an Agilent 5977A mass spectrometer (MS) operating under

electron impact ionization at 70 eV. The MS source was held at 230°C and the quadrupole at 150 °C and helium was used as carrier gas. The GC oven was held at 100°C for 2 min, increased to 300 °C at 10 °C/min and held for 4 min, and held at 325°C for 3 min.

RAB5 immunostaining and fluorescence microscopy

Cells were plated on 12-well plates containing cover glass coverslips for 4 days in the presence of doxycycline or small molecule treatments as indicated in the text. Medium was changed on day 2. Media was supplemented with 20 µM dynasore (Cat. #D7693, Sigma Millipore) 3 h. To visualize RAB5 positive endosomes, cells were fixed with ice-cold 4% paraformaldehyde solution (Cat. #J19943-K2, Thermo Scientific), washed three times with 0.1% Tween-20 in PBS (PBST) before incubation with 0.2% Triton-X100 for 10 min. Cells were then washed 3 times with PBST (each 5 min), incubated with 8% BSA in PBST (Cat. #700-100P, Gemini Bio-Products) for 20 min, and washed three times with PBST (each 5 min). Cells were then incubated with primary anti-RAB5 antibody at 4 °C overnight diluted in 8% BSA in PBST (1:500 dilution, Cat. #3547, lot 7, Cell Signaling Technology). Secondary anti-rabbit Alexa Fluor 568 antibody (1:1000 dilution, Cat. #A-11011, Life Technologies) and Hoechst (1:1000 dilution, Cat. #4082, Cell Signaling Technology) diluted in 8% BSA PBST were applied for 2 h at room temperature followed by an incubation of HCS Cell Mask Deep Red Stain (Cat. #H32721, Invitrogen) for 30 min at room temperature. Cells were then washed three times with PBST (5 min each). Antibodies were validated for human reactivity by the manufacturer and used per their instructions. Coverslips were mounted with Fluoromount-G (Cat. #0100-01, Southern Biotech) on microscopy plates (Cat. #12-544-7, Thermo Fisher Scientific), and sealed with nail polish (Cat. #88-128, Genesee Scientific Corp.)

Cells were imaged using a 60x Plan Apo 1.4 NA objective on a Nikon Ti2-E microscope with a Yokogawa X1 spinning disk confocal system, MLC400B 4-line (405nm, 488nm, 561nm, and 647nm) dual-fiber laser combiner (Agilent), Prime 95B back-thinned sCMOS camera (Teledyne Photometrics), piezo Z-stage (Mad City Labs) and running NIS Elements software. To separate the emission of individual flours, band-pass emission filters were used for each channel (450/50, 525/36, 605/52, and 705/72). Background fluorescence

intensity was corrected for each image. One representative image is depicted per experimental condition. RAB5 was quantified using ImageJ 1.53k with n cell number as depicted in each figure.

Liquid chromatograph - Mass spectrometry (LC-MS), sample preparation, and sphingolipid analysis

For targeted sphingolipid analysis, cells were washed with 0.9% (w/v) NaCl and extracted with 0.25 mL of −20°C methanol, 0.25 mL -20°C chloroform, and 0.1 mL of water spiked with deuterated internal standards (20 picomoles of D7- sphinganine (Avanti, Croda International Plc, 860658), 2 picomoles of D3-deoxysphinganine (Avanti, Croda International Plc, 860474), 200 picomoles of C15 ceramide-d7 (d18:1-d7/15:0) (Avanti, Croda International Plc, 860681), 100 picomoles of C13-dihydroceramide-d7 (d18:0-d7/13:0) (Avanti, Croda International Plc, 330726)). The tubes were vortexed for 5 min, centrifuged at 20,000 x *g* at 4°C for 5 min, and the lower organic phase was collected. The remaining polar phase was re-extracted with 2 µL formic acid and 0.25 mL of -20 °C chloroform. The organic phases were combined, dried under air, resuspended in 80 µL Buffer B (0.2% formic acid and 1 mM ammonium formate in methanol), sonicated for 10 min, and centrifuged for 10 min at 20,000 x *g* at 4 °C. Ceramide species in the supernatant were quantified using LC-MS (Agilent 6460 QQQ, MassHunter LC/MS Acquisition (v.B.08.02)) equipped with a C8 column (Spectra 3 µm C8SR 150 × 3 mm inner diameter, Peeke Scientific) as previously described (Bielawski et al., 2009) with mobile phase A (2 mM ammonium formate and 0.2% formic acid in HPLC grade water) and mobile phase B (0.2% formic acid and 1 mM ammonium formate in methanol). The gradient elution program consisted of the following profile: 0 min, 82% B; 3 min, 82% B; 4 min, 90% B, 18 min, 99% B; 25 min, 99%, 27 min, 82% B, 30 min, 82% B. Column re-equilibration followed each sample and lasted 10 min. The capillary voltage was set to 3.5 kV, the drying gas temperature was 350 °C, the drying gas flow rate was 10 L/min and the nebulizer pressure was 60 psi. Ceramide species were analyzed by selective reaction monitoring of the transition from precursor to product ions at associated optimized collision energies and fragmentor voltages are provided elsewhere (10). SL and deoxySL species were then quantified from spiked internal standards and normalized to protein content.

To quantify labeling on SL and deoxySL species from [U-$^{13}C_{16}$]palmitate a Q Exactive orbitrap mass spectrometer with a Vanquish Flex Binary UHPLC system (Thermo Scientific) was used with a Kinetex 2.6 µM C8 100 Å 150 x 3 mm LC column (Phenomenex) at 40°C. 5 µL of sample was injected. Chromatography was performed using a gradient of 2 mM ammonium formate and 0.2 % formic acid (mobile phase A) and 1 mM ammonium formate and 0.2 % formic acid in methanol (mobile phase B), at a flow rate of 0.5 mL/min. The LC gradient held at 82% B for 0-3 min, then ran from 82%-90% B in 3-4 min, then 90-99% in 4-18 min, held at 99% B for 7 min, then reduced from 99%-82% from 25-27 min, then held at 82% for a further 13 mins. Lipids were analyzed in positive mode using spray voltage 3 kV. Sweep gas flow was 5 arbitrary units, auxiliary gas flow 7 arbitrary units and sheath gas flow 50 arbitrary units, with a capillary temperature of 300°C. Full MS (scan range 150-2000 m/z) was used at 70 000 resolution with $1e^6$ automatic gain control and a maximum injection time of 200 ms. Data dependent MS2 (Top 6) mode at 17 500 resolution with automatic gain control set at $1e^5$ with a maximum injection time of 50 ms was used for peak identification, combined with known standards where possible.

Statistics

Data visualization and statistical analysis were performed using GraphPad Prism (v9.1.0) and Adobe Illustrator CS6 (v.16.0.0). The type and number of replicates and the statistical test used are described in each figure legends. Data are presented as means ± s.e.m. or box (25th to 75th percentile with median line) and whiskers (min. to max. values). Tissue culture was conducted in 12-well tissue culture plates for metabolic studies, 6-well tissue culture plates for soft agar colony formation assay, and 96-well culture plates for Seahorse analysis and growth responses (PrestoBlue assay). Each culture well was considered as a cellular replicate for a given preparation. One representative figure per condition is depicted for confocal microscopy analysis. *P* values were calculated using a two-sided Student's *t*-test, one-way ANOVA or two-way ANOVA, and nested- analysis was performed as indicated, with $*P < 0.05$; $**P < 0.01$; $***P < 0.001$, and $****P < 0.0001$ as indicated in each figure legend.

Data availability:

The datasets generated and analyzed during the current study are available in the article and are available from the corresponding author upon reasonable request.

Competing interests. The authors declare that they have no conflict of interest with the contents of this article.

Acknowledgments: We thank the Nikon Imaging Center at UC San Diego, where we collected imaging data.

Authors' contribution.

C.M.M. and T.C. designed the study. T.C. performed *in vitro* cell studies and targeted metabolomics. T.C., T.M., and J.G. engineered *SPTLC1* expression cells. T.M. performed time-dependent spheroid experiments. T.C. and G.H.MG. performed high-resolution mass spectrometry. T.C. and R.S.K. performed fluorescence imaging experiments. T.C. and S.V.K. performed soft agar growth assays. T.C. analyzed data and prepared figures. C.M.M. and T.C. wrote the manuscript with input from all authors.

References

1. Hannun YA, Obeid LM. Sphingolipids and their metabolism in physiology and disease. Vol. 19, Nature Reviews Molecular Cell Biology. Nature Publishing Group; 2018. p. 175–91.
2. Penno A, Reilly MM, Houlden H, Laurá M, Rentsch K, Niederkofler V, et al. Hereditary Sensory Neuropathy Type 1 Is Caused by the Accumulation of Two Neurotoxic Sphingolipids. Journal of Biological Chemistry. 2010 Apr 9;285(15):11178–87.
3. Lone MA, Santos T, Alecu I, Silva LC, Hornemann T. 1-Deoxysphingolipids. Vol. 1864, Biochimica et Biophysica Acta - Molecular and Cell Biology of Lipids. Elsevier B.V.; 2019. p. 512–21.
4. Zitomer NC, Mitchell T, Voss KA, Bondy GS, Pruett ST, Garnier-Amblard EC, et al. Ceramide synthase inhibition by fumonisin B1 causes accumulation of 1-deoxysphinganine. A novel category of bioactive 1-deoxysphingoid bases and 1-deoxydihydroceramides biosynthesized by mammalian cell lines and animals. Journal of Biological Chemistry [Internet]. 2009 Feb 20 [cited 2021 May 23];284(8):4786–95. Available from: https://pubmed.ncbi.nlm.nih.gov/19095642/
5. Schwartz NU, Mileva I, Gurevich M, Snider J, Hannun YA, Obeid LM. Quantifying 1-deoxydihydroceramides and 1-deoxyceramides in mouse nervous system tissue. Prostaglandins and Other Lipid Mediators. 2019 Apr 1;141:40–8.
6. Ferreira CR, Goorden SMI, Soldatos A, Byers HM, Ghauharali-van der Vlugt JMM, Beers-Stet FS, et al. Deoxysphingolipid precursors indicate abnormal sphingolipid metabolism in individuals with primary and secondary disturbances of serine availability. Molecular Genetics and Metabolism. 2018 Jul 1;124(3):204–9.
7. Esaki K, Sayano T, Sonoda C, Akagi T, Suzuki T, Ogawa T, et al. L-serine deficiency elicits intracellular accumulation of cytotoxic deoxysphingolipids and lipid body formation. Journal of Biological Chemistry [Internet]. 2015 Jun 5 [cited 2020 Dec 31];290(23):14595–609. Available from: https://pubmed.ncbi.nlm.nih.gov/25903138/

8. Alecu I, Tedeschi A, Behler N, Wunderling K, Lamberz C, Lauterbach MAR, et al. Localization of 1-deoxysphingolipids to mitochondria induces mitochondrial dysfunction. Journal of Lipid Research [Internet]. 2017 Jan 1 [cited 2021 May 23];58(1):42–59. Available from: https://pubmed.ncbi.nlm.nih.gov/27881717/

9. Oswald MCW, West RJH, Lloyd-Evans E, Sweeney ST. Identification of dietary alanine toxicity and trafficking dysfunction in a Drosophila model of hereditary sensory and autonomic neuropathy type 1. Human molecular genetics [Internet]. 2015 [cited 2022 Jan 12];24(24):6899–909. Available from: https://pubmed.ncbi.nlm.nih.gov/26395456/

10. Muthusamy T, Cordes T, Handzlik MK, You L, Lim EW, Gengatharan J, et al. Serine restriction alters sphingolipid diversity to constrain tumour growth. Nature [Internet]. 2020 [cited 2020 Aug 13];586(7831). Available from: http://www.nature.com/articles/s41586-020-2609-x

11. Kory N, Wyant GA, Prakash G, de Bos J uit, Bottanelli F, Pacold ME, et al. SFXN1 is a mitochondrial serine transporter required for one-carbon metabolism. Science [Internet]. 2018 Nov 16 [cited 2021 Nov 11];362(6416). Available from: https://www.science.org/doi/abs/10.1126/science.aat9528

12. Labuschagne CF, van den Broek NJF, Mackay GM, Vousden KH, Maddocks ODK. Serine, but not glycine, supports one-carbon metabolism and proliferation of cancer cells. Cell Reports [Internet]. 2014 May 22 [cited 2021 Dec 18];7(4):1248–58. Available from: http://www.cell.com/article/S2211124714003477/fulltext

13. Reid MA, Allen AE, Liu S, Liberti M v., Liu P, Liu X, et al. Serine synthesis through PHGDH coordinates nucleotide levels by maintaining central carbon metabolism. Nature Communications 2018 9:1 [Internet]. 2018 Dec 21 [cited 2021 Nov 11];9(1):1–11. Available from: https://www.nature.com/articles/s41467-018-07868-6

14. Li X, Gracilla D, Cai L, Zhang M, Yu X, Chen X, et al. ATF3 promotes the serine synthesis pathway and tumor growth under dietary serine restriction. Cell reports [Internet]. 2021 Sep 21 [cited 2021 Dec 18];36(12). Available from: https://pubmed.ncbi.nlm.nih.gov/34551291/

15. Fan J, Ye J, Kamphorst JJ, Shlomi T, Thompson CB, Rabinowitz JD. Quantitative flux analysis reveals folate-dependent NADPH production. Nature [Internet]. 2014 [cited 2021 Dec 18];510(7504):298. Available from: /pmc/articles/PMC4104482/

16. Lewis CA, Parker SJ, Fiske BP, McCloskey D, Gui DY, Green CR, et al. Tracing compartmentalized NADPH metabolism in the cytosol and mitochondria of mammalian cells. Molecular cell. 2014 Jul 17;55(2):253–63.

17. Yang L, Garcia Canaveras JC, Chen Z, Wang L, Liang L, Jang C, et al. Serine Catabolism Feeds NADH when Respiration Is Impaired. Cell Metabolism [Internet]. 2020 Apr 7 [cited 2021 Dec 18];31(4):809-821.e6. Available from: http://www.cell.com/article/S1550413120301145/fulltext

18. Gao X, Lee K, Reid MA, Sanderson SM, Qiu C, Li S, et al. Serine Availability Influences Mitochondrial Dynamics and Function through Lipid Metabolism. Cell reports [Internet]. 2018 Mar 27 [cited 2021 Nov 11];22(13):3507–20. Available from: https://pubmed.ncbi.nlm.nih.gov/29590619/

19. Lauterbach MA, Saavedra V, Mangan MSJ, Penno A, Thiele C, Latz E, et al. 1-Deoxysphingolipids cause autophagosome and lysosome accumulation and trigger NLRP3 inflammasome activation. https://doi.org/101080/1554862720201804677 [Internet]. 2020 [cited 2021 Oct 19];17(8):1947–61. Available from: https://www.tandfonline.com/doi/abs/10.1080/15548627.2020.1804677

20. Karsai G, Steiner R, Kaech A, Lone MA, von Eckardstein A, Hornemann T. Metabolism of HSAN1- and T2DM-associated 1-deoxy-sphingolipids inhibits the migration of fibroblasts. Journal of Lipid Research. 2021 Jan 1;62:100122.

21. Truman JP, Ruiz CF, Trayssac M, Mao C, Hannun YA, Obeid LM. Sphingosine kinase 1 downregulation is required for adaptation to serine deprivation. FASEB journal : official publication of the Federation of American Societies for Experimental Biology [Internet]. 2021 Feb 1 [cited 2021 Dec 18];35(2). Available from: https://pubmed.ncbi.nlm.nih.gov/33484475/

22. Truman J-P, Ruiz CF, Montal E, Garcia-Barros M, Mileva I, Snider AJ, et al. 1-deoxysphinganine initiates adaptive responses to serine and glycine starvation in cancer cells via proteolysis of sphingosine kinase. Journal of Lipid Research [Internet]. 2021 Nov [cited 2021 Nov 29];0(0):100154. Available from: http://www.jlr.org/article/S0022227521001371/fulltext

23. Hannich JT, Haribowo AG, Gentina S, Paillard M, Gomez L, Pillot B, et al. 1-Deoxydihydroceramide causes anoxic death by impairing chaperonin-mediated protein folding. Nature Metabolism. 2019 Oct 1;1(10):996–1008.

24. Lim EW, Handzlik MK, Trefts E, Gengatharan JM, Pondevida CM, Shaw RJ, et al. Progressive alterations in amino acid and lipid metabolism correlate with peripheral neuropathy in PolgD257A mice. Science advances [Internet]. 2021 Oct 1 [cited 2021 Nov 11];7(42). Available from: https://pubmed.ncbi.nlm.nih.gov/34652935/

25. Othman A, Bianchi R, Alecu I, Wei Y, Porretta-Serapiglia C, Lombardi R, et al. Lowering plasma 1-deoxysphingolipids improves neuropathy in diabetic rats. Diabetes. 2015 Mar;64(3):1035–45.

26. Fridman V, Zarini S, Sillau S, Harrison K, Bergman BC, Feldman EL, et al. Altered plasma serine and 1-deoxydihydroceramide profiles are associated with diabetic neuropathy in type 2 diabetes and obesity. Journal of Diabetes and its Complications. 2021 Apr 1;35(4).

27. Eichler FS, Hornemann T, McCampbell A, Kuljis D, Penno A, Vardeh D, et al. Overexpression of the wild-type SPT1 subunit lowers desoxysphingolipid levels and rescues the phenotype of HSAN1. Journal of Neuroscience. 2009 Nov 18;29(46):14646–51.

28. Bode H, Bourquin F, Suriyanarayanan S, Wei Y, Alecu I, Othman A, et al. HSAN1 mutations in serine palmitoyltransferase reveal a close structure-function-phenotype relationship. Human molecular genetics [Internet]. 2016 Mar 1 [cited 2021 Nov 11];25(5):853–65. Available from: https://pubmed.ncbi.nlm.nih.gov/26681808/

29. Gable K, Gupta SD, Han G, Niranjanakumari S, Harmon JM, Dunn TM. A Disease-causing Mutation in the Active Site of Serine Palmitoyltransferase Causes Catalytic Promiscuity *. Journal

of Biological Chemistry [Internet]. 2010 Jul 23 [cited 2021 Dec 18];285(30):22846–52. Available from: http://www.jbc.org/article/S0021925820603258/fulltext

30. Hines TJ, Tadenev ALD, Lone MA, Hatton CL, Bagasrawala I, Stum MG, et al. Precision mouse models of Yars/dominant intermediate Charcot-Marie-Tooth disease type C and Sptlc1/hereditary sensory and autonomic neuropathy type 1. Journal of Anatomy [Internet]. 2021 Dec 7 [cited 2021 Dec 18]; Available from: https://onlinelibrary.wiley.com/doi/full/10.1111/joa.13605

31. Badur MG, Zhang H, Metallo CM. Enzymatic passaging of human embryonic stem cells alters central carbon metabolism and glycan abundance. Biotechnology journal [Internet]. 2015 Oct 1 [cited 2021 Nov 13];10(10):1600–11. Available from: https://pubmed.ncbi.nlm.nih.gov/26289220/

32. Jiang L, Shestov AA, Swain P, Yang C, Parker SJ, Wang QA, et al. Reductive carboxylation supports redox homeostasis during anchorage-independent growth. Nature [Internet]. 2016 Apr 14 [cited 2021 Nov 13];532(7598):255–8. Available from: https://pubmed.ncbi.nlm.nih.gov/27049945/

33. Grimes DR, Kelly C, Bloch K, Partridge M. A method for estimating the oxygen consumption rate in multicellular tumour spheroids. Journal of The Royal Society Interface [Internet]. 2014 Mar 6 [cited 2021 Dec 18];11(92). Available from: https://royalsocietypublishing.org/doi/abs/10.1098/rsif.2013.1124

34. Eales KL, Hollinshead KER, Tennant DA. Hypoxia and metabolic adaptation of cancer cells. Oncogenesis [Internet]. 2016 Jan [cited 2021 Dec 18];5(1):e190. Available from: /pmc/articles/PMC4728679/

35. Karsai G, Lone M, Kutalik Z, Thomas Brenna J, Li H, Pan D, et al. FADS3 is a Δ14Z sphingoid base desaturase that contributes to gender differences in the human plasma sphingolipidome. Journal of Biological Chemistry. 2020;295(7):1889–97.

36. Clark AJ, Kugathasan U, Baskozos G, Priestman DA, Fugger N, Lone MA, et al. An iPSC model of hereditary sensory neuropathy-1 reveals L-serine-responsive deficits in neuronal ganglioside composition and axoglial interactions. Cell Reports Medicine. 2021 Jul 20;2(7):100345.

37. Shimeno H, Soeda S, Sakamoto M, Kouchi T, Kowakame T, Kihara T. Partial purification and characterization of sphingosine N-acyltransferase (ceramide synthase) from bovine liver mitochondrion-rich fraction. Lipids [Internet]. 1998 [cited 2022 Jan 17];33(6):601–5. Available from: https://pubmed.ncbi.nlm.nih.gov/9655376/

38. Zigdon H, Kogot-Levin A, Park JW, Goldschmidt R, Kelly S, Merrill AH, et al. Ablation of Ceramide Synthase 2 Causes Chronic Oxidative Stress Due to Disruption of the Mitochondrial Respiratory Chain *. Journal of Biological Chemistry [Internet]. 2013 Feb 1 [cited 2022 Jan 17];288(7):4947–56. Available from: http://www.jbc.org/article/S0021925820462969/fulltext

39. Dany M, Ogretmen B. Ceramide induced mitophagy and tumor suppression. Biochimica et Biophysica Acta (BBA) - Molecular Cell Research. 2015 Oct 1;1853(10):2834–45.

40. Maddocks ODK, Athineos D, Cheung EC, Lee P, Zhang T, van den Broek NJF, et al. Modulating the therapeutic response of tumours to dietary serine and glycine starvation. Nature [Internet]. 2017 Apr 19 [cited 2021 Jan 4];544(7650):372–6. Available from: https://www.nature.com/articles/nature22056

41. Wu J, Ma S, Sandhoff R, Ming Y, Hotz-Wagenblatt A, Timmerman V, et al. Loss of Neurological Disease HSAN-I-Associated Gene SPTLC2 Impairs CD8 + T Cell Responses to Infection by Inhibiting T Cell Metabolic Fitness. Immunity [Internet]. 2019 May 21 [cited 2022 Jan 12];50(5):1218-1231.e5. Available from: https://pubmed.ncbi.nlm.nih.gov/30952607/

42. Houlden H, King R, Blake J, Groves M, Love S, Woodward C, et al. Clinical, pathological and genetic characterization of hereditary sensory and autonomic neuropathy type 1 (HSAN I). Brain [Internet]. 2006 Feb 1 [cited 2022 Jan 12];129(2):411–25. Available from: https://academic.oup.com/brain/article/129/2/411/292263

43. Sousa LP, Lax I, Shen H, Ferguson SM, de Camilli P, Schlessinger J. Suppression of EGFR endocytosis by dynamin depletion reveals that EGFR signaling occurs primarily at the plasma membrane. Proceedings of the National Academy of Sciences of the United States of America

[Internet]. 2012 Mar 20 [cited 2022 Jan 12];109(12):4419–24. Available from: https://www.pnas.org/content/109/12/4419

44. Gantner ML, Eade K, Wallace M, Handzlik MK, Fallon R, Trombley J, et al. Serine and Lipid Metabolism in Macular Disease and Peripheral Neuropathy. New England Journal of Medicine [Internet]. 2019 [cited 2019 Oct 4];381(15). Available from: http://www.ncbi.nlm.nih.gov/pubmed/31509666

45. Mosesson Y, Mills GB, Yarden Y. Derailed endocytosis: an emerging feature of cancer. Nature Reviews Cancer 2008 8:11 [Internet]. 2008 Nov [cited 2022 Jan 17];8(11):835–50. Available from: https://www.nature.com/articles/nrc2521

46. Young JD. INCA: a computational platform for isotopically non-stationary metabolic flux analysis. Bioinformatics (Oxford, England). 2014 May 1;30(9):1333–5.

47. Cordes T, Metallo CM. Quantifying Intermediary Metabolism and Lipogenesis in Cultured Mammalian Cells Using Stable Isotope Tracing and Mass Spectrometry. In: Methods in molecular biology (Clifton, NJ). 2019. p. 219–41.

48. Melamud E, Vastag L, Rabinowitz JD. Metabolomic analysis and visualization engine for LC - MS data. Analytical Chemistry. 2010 Dec 1;82(23):9818–26.

FIGURE LEGENDS:

Figure 1: Alanine promotes deoxySL synthesis and compromises early spheroid formation

A. Total deoxyDHCer, deoxyCer, DHCer, and Cer levels in HCT116 cells cultured with increasing alanine for 3 days relative to 0 mM alanine.
B. Alanine levels in HCT116 cells cultured for 3 days with 1 mM alanine and 5 µM UK5099. Schematic depicting alanine involved in mitochondrial and sphingolipid metabolism. SPT: serine palmitoyltransferase; MPC: mitochondrial pyruvate carrier
C. DeoxySA m18:0 levels in HCT116 cells cultured for 3 days with 1 mM alanine and 5 µM UK5099.
D. Levels of deoxyDHCer species in HCT116 cells cultured for 3 days with 1mM alanine and 5 µM UK5099.
E. Adherent cell growth of HCT116 cells cultured with increasing alanine concentrations for 3 days.
F. Schematic depicting spheroid formation assay with inhibitors targeting MPC (UK5099), SPT (myriocin), and ceramide synthase (CERS, fumonisin B1).
G. HCT116 spheroid growth with DMSO, 1 mM alanine, 5 µM UK5099, 10 nM myriocin, 10 µM fumonisin B1 (FeB1) for 3 to 8 days as indicated in the figure.

Data are presented as means ± s.e.m. (A-D, G) with three cellular replicates or box (25th to 75th percentile with median line) and whiskers (min. to max. values) (E) with five cellular replicates. One-way ANOVA (B, C) or two-way ANOVA (A, D, G). Significance in A is compared to 0mM alanine. Significance for D and G is compared to DMSO. Results are depicted from one representative experiment and each experiment was repeated independently three times with similar results. * $P < 0.05$, ** $P < 0.01$, *** $P < 0.001$, **** $P < 0.0001$.

Figure 2: Mutant *SPTLC1*^{C133W} drives non-canonical deoxySL biosynthesis.

A. Schematic depicting serine palmitoyl transferase (SPT) promiscuity catalyzing sphingolipid (SL) species from serine or deoxy-sphingolipids (deoxySL) from alanine. Mutant *SPTLC1*^{C133W} (C133W, red) has an increased affinity for alanine as substrate compared to *SPTLC1*^{WT} (WT, grey) driving deoxySL synthesis.
B. Immunoblotting of SPTLC1 and actin in SPT expressing HCT116 cell lines with doxycycline for 4 days.
C. Total DHCer, Cer, deoxyDHCer, and deoxyCer levels in HCT116 cells expressing *SPTLC1*^{WT} or *SPTLC1*^{C133W} cultured for 5 days with increasing doxycycline concentrations.
D. Levels of deoxyDHCer species in engineered SPT HCT116 cells cultured for 5 days with 0.1 µg/ml doxycycline.
E. Levels of deoxyCer species in engineered SPT HCT116 cells cultured for 5 days with 0.1 µg/ml doxycycline.

Data are presented as means ± s.e.m. with three cellular replicates. Two-way ANOVA compared to 0 µg/ml doxycycline (C) or Student's t-test (D, E). Experiments were repeated two (B) or three (C-E) times with similar results. *$P < 0.05$, ** $P < 0.01$, *** $P < 0.001$, **** $P < 0.0001$.

Figure 3: Impact of deoxySL synthesis on metabolic pathways

A. Schematic depicting trace into SL and deoxySL in engineered HCT116 cell lines cultured with 0.1 µg/ml doxycycline for 7 days prior tracing with [U-$^{13}C_{16}$]palmitate for 15min, 1h, and 4h.
B. Label on canonical SLs from ^{13}C palmitate tracer.
C. Label on non-canonical SLs from ^{13}C palmitate tracer.
D. Label on citrate from ^{13}C palmitate tracer.
E. Adherent cell growth of *SPT* expressing HCT116 cell lines cultured for 3 days with increasing doxycycline concentrations.
F. Spheroid growth in HCT116 *SPT* expressing cell lines with 0.1 µg/ml doxycycline.
G. DeoxyDHCer m18:0/16:0 levels in HCT116 *SPTLC1*^{C133W} expressing cells cultured for 3 days with alanine, doxycycline, or 100 nM deoxySA m18:0.

Data are presented as means ± s.e.m. with three cellular replicates (B, C, D, G) or box (25th to 75th percentile with median line) and whiskers (min. to max. values) (E, F). Student's *t*-test (B, D), nested *t*-test (F), or one-way ANOVA (G). Experiments in E, F, and G were repeated three times with similar results. Data in F depict average of 3 independent experiments with each 3 cellular replicates. *$P < 0.05$, ** $P < 0.01$, *** $P < 0.001$, **** $P < 0.0001$

Figure 4: Alanine and deoxySL synthesis influence colony formation in soft agar

A. Colony formation in HCT116 wildtype (WT, grey) and mutant (C133W, red) *SPTLC1* expressing cells cultured for 7 days with 0.1 µg/ml doxycycline.
B. Colony formation in *SPTLC1* HCT116 cells with 10nM myriocin cultured for 7 days with 0.1 µg/ml doxycycline.
C. Colony formation in HCT116 cells with 1 mM alanine and 10 nM myriocin or 5 µM UK5099 cultured for 7 days with 0.1 µg/ml doxycycline.
D. Colony formation in HCT116 cells with 1 mM alanine and 1mM serine cultured for 7 days.

Data are presented as box (25th to 75th percentile with median line) and whiskers (min. to max. values) obtained from three independent experiments with each three cellular replicates. Nested *t*-test (A) or nested one-way ANOVA (B-D) with *$P < 0.05$, ** $P < 0.01$, *** $P < 0.001$, ****$P < 0.0001$.

Figure 5: DeoxySLs compromise endocytosis.

A. RAB5 immunostaining with *SPTLC1*^{WT} and *SPTLC1*^{C133W} expressing HCT116 cultured for 4 days with 0.1 µg/ml doxycycline. Dynasore (dyn) was given with 20 µM for 3h.
B. RAB5 immunostaining with *SPTLC1*^{WT} and *SPTLC1*^{C133W} expressing A549 cultured for 4 days with 1 µg/ml doxycycline. Dynasore (dyn) was given with 20 µM for 3h.
C. RAB5 immunostaining with HCT116 cells cultured with 1mM alanine or 1mM serine.

Violin blots depict relative RAB5 intensity obtained from n= cell number. Data are representative of two independent experiments. White scale bar indicates 10 µm.

Figure 6: Schematic metabolic concept depicting metabolic impact of plasma membrane endocytosis through the lipidome compromising anchorage independent cell growth. SPT – serine palmitoyltransferase.

Supplementary Figure 1: Alanine promotes deoxySL synthesis

A. Schematic depicting [2,3-^{13}C]alanine trace into TCA cycle metabolism. Open circles represent ^{12}C, closed circles ^{13}C atoms. Percent label on TCA cycle intermediates in HCT116 cells cultured with UK5099 and ^{13}C alanine for 24h.
B. Levels of deoxyCer species in HCT116 cells cultured for 3 days with 1mM alanine and 5 µM UK5099.
C. Total deoxyDHCer, deoxyCer, DHCer, and Cer levels in A549 cells cultured with increasing alanine for 3 days relative to 0 mM alanine.
D. Adherent cell growth of A549 cells cultured with increasing alanine concentrations for 3 days.

Data are presented as means ± s.e.m. (B, C) or box (25th to 75th percentile with median line) and whiskers (min. to max. values) (A, D) with three (A, B, C) or five (D) cellular replicates. Student's t-test (A) or two-way ANOVA (B, C). Significance in A is compared to 0mM alanine. Significance in B is compared to DMSO control condition. Results are depicted from one representative experiment and each experiment was repeated independently three times with similar results. * $P < 0.05$, ** $P < 0.01$, *** $P < 0.001$, **** $P < 0.0001$.

Supplementary Figure 2: Mutant *SPTLC1* drives non-canonical deoxySL biosynthesis

A. DeoxySA levels in SPT expressing HCT116 cells.

B. Levels of DHCer species in HCT116 cell lines.

C. Levels of Cer species in HCT116 cell lines.

Cells were cultured for 5 days with 0.1 µg/ml doxycycline. Data are presented as means ± s.e.m. with three cellular replicates. Results are depicted from one representative experiment and each experiment was repeated independently three times with similar results. Two-way ANOVA (A) relative to 0µg/ml doxycycline or Students *t*-test (B,C) with *$P < 0.05$, ** $P < 0.01$, *** $P < 0.001$, **** $P < 0.0001$.

Supplementary Figure 3: Impact of deoxySL synthesis on metabolic pathways

A. Percent label on deoxyDHCer m18:0/16:0 from ^{13}C palmitate tracer in HCT116 *SPTLC1*^{C133W} expressing cells.

B. Percent label on DHCer d18:0/16:0 from ^{13}C palmitate tracer in HCT116 *SPTLC1*^{C133W} expressing cells.

C. Atom transition map depicting [U-$^{13}C_6$]glucose oxidation with ^{12}C (open circles) and ^{13}C (closed circles) carbons into TCA cycle. Labeling on metabolites in SPT expressing HCT116 cells cultured for 4d with 0.1 µg/ml doxycycline followed by 48h trace with [U-$^{13}C_6$]glucose.

D. Oxygen consumption (OCR) in HCT116 SPTLC1^{C133W} cells cultured for 6 days with increasing doxycycline concentrations.

E. DeoxyDHCer species in HCT116 *SPTLC1*^{C133W} cells cultured for 3 days with doxycycline, alanine or deoxySA m18:0.

F. Levels of total sphingolipid species in HCT116 *SPTLC1*^{C133W} cells cultured for 3 days with doxycycline, alanine, and deoxySA m18:0.

Data are presented as means ± s.e.m. with three (A-C, E, G) or five (D) cellular replicates. Results are depicted from one representative experiment and each experiment was repeated independently two or more times with similar results. Results in A and B were obtained from one independent experiment. Students *t*-test with *$P < 0.05$, ** $P < 0.01$, *** $P < 0.001$.

Supplementary Figure 4: Impact of deoxySL synthesis on colony formation in A549 cells

A. Immunoblotting of SPTLC1 and actin in SPT expressing A549 cells with doxycycline for 4 days.
B. Levels of deoxyDHCer species in engineered A549 cells cultured for 4 days with 1 µg/ml doxycycline.
C. Colony formation in engineered A549 cells cultured for 14 days with 10 nM myriocin (Myr) and 1 µg/ml doxycycline.
D. Colony formation in A549 cells cultured for 14 days with 1 mM alanine and 10 nM myriocin.

Data are presented as means ± s.e.m. with three cellular replicates (B). Data in C and D are presented as box (25th to 75th percentile with median line) and whiskers (min. to max. values) obtained from three independent experiments with each three cellular replicates. Student's t-test (B) or nested one-way ANOVA (C, D). *$P < 0.05$, ** $P < 0.01$, *** $P < 0.001$, **** $P < 0.0001$

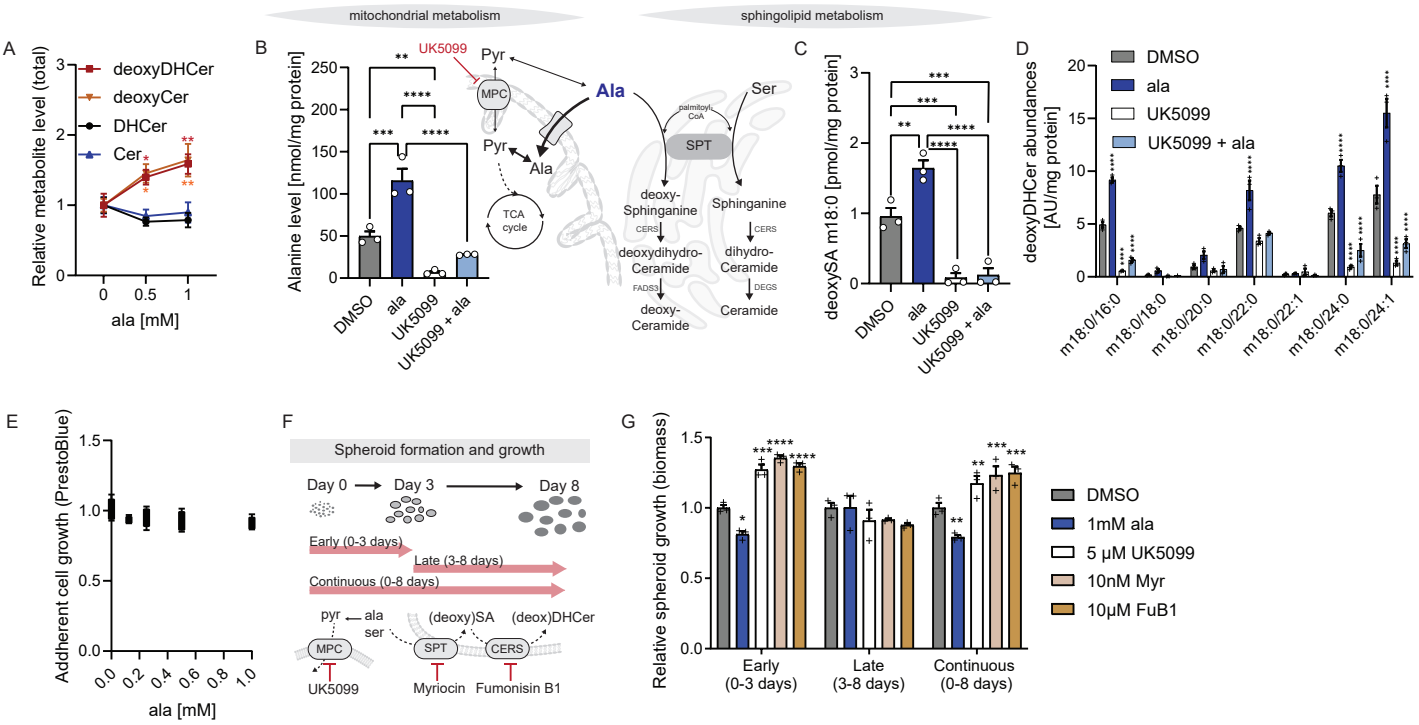

Figure 1: Alanine promotes deoxySL synthesis and compromises early spheroid formation

A. Total deoxyDHCer, deoxyCer, DHCer, and Cer levels in HCT116 cells cultured with increasing alanine for 3 days relative to 0 mM alanine.
B. Alanine levels in HCT116 cells cultured for 3 days with 1 mM alanine and 5 µM UK5099. Schematic depicting alanine involved in mitochondrial and sphingolipid metabolism. SPT: serine palmitoyltransferase; MPC: mitochondrial pyruvate carrier
C. DeoxySA m18:0 levels in HCT116 cells cultured for 3 days with 1 mM alanine and 5 µM UK5099.
D. Levels of deoxyDHCer species in HCT116 cells cultured for 3 days with 1mM alanine and 5 µM UK5099.
E. Adherent cell growth of HCT116 cells cultured with increasing alanine concentrations for 3 days.
F. Schematic depicting spheroid formation assay with inhibitors targeting MPC (UK5099), SPT (myriocin), and ceramide synthase (CERS, fumonisin B1).
G. HCT116 spheroid growth with DMSO, 1 mM alanine, 5 µM UK5099, 10 nM myriocin, 10 µM fumonisin B1 (FeB1) for 3 to 8 days as indicated in the figure.

Data are presented as means ± s.e.m. (A-D, G) with three cellular replicates or box (25th to 75th percentile with median line) and whiskers (min. to max. values) (E) with five cellular replicates. One-way ANOVA (B, C) or two-way ANOVA (A, D, G). Significance in A is compared to 0mM alanine. Significance for D and G is compared to DMSO. Results are depicted from one representative experiment and each experiment was repeated independently three times with similar results. * $P < 0.05$, ** $P < 0.01$, *** $P < 0.001$, **** $P < 0.0001$.

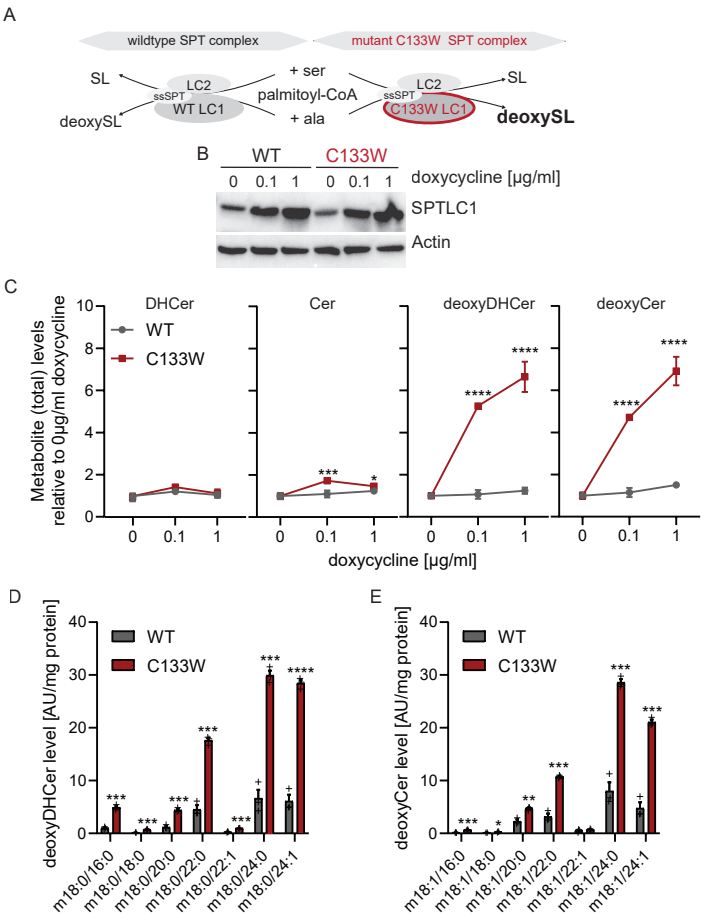

Figure 2: Mutant *SPTLC1*^{C133W} drives non-canonical deoxySL biosynthesis.

A. Schematic depicting serine palmitoyl transferase (SPT) promiscuity catalyzing sphingolipid (SL) species from serine or deoxy-sphingolipids (deoxySL) from alanine. Mutant *SPTLC1*^{C133W} (C133W, red) has an increased affinity for alanine as substrate compared to *SPTLC1*^{WT} (WT, grey) driving deoxySL synthesis.
B. Immunoblotting of SPTLC1 and actin in SPT expressing HCT116 cell lines with doxycycline for 4 days.
C. Total DHCer, Cer, deoxyDHCer, and deoxyCer levels in HCT116 cells expressing *SPTLC1*^{WT} or *SPTLC1*^{C133W} cultured for 5 days with increasing doxycycline concentrations.
D. Levels of deoxyDHCer species in engineered SPT HCT116 cells cultured for 5 days with 0.1 µg/ml doxycycline.
E. Levels of deoxyCer species in engineered SPT HCT116 cells cultured for 5 days with 0.1 µg/ml doxycycline.

Data are presented as means ± s.e.m. with three cellular replicates. Two-way ANOVA compared to 0 µg/ml doxycycline (C) or Student's t-test (D, E). Experiments were repeated two (B) or three (C-E) times with similar results. *$P < 0.05$, ** $P < 0.01$, *** $P < 0.001$, **** $P < 0.0001$.

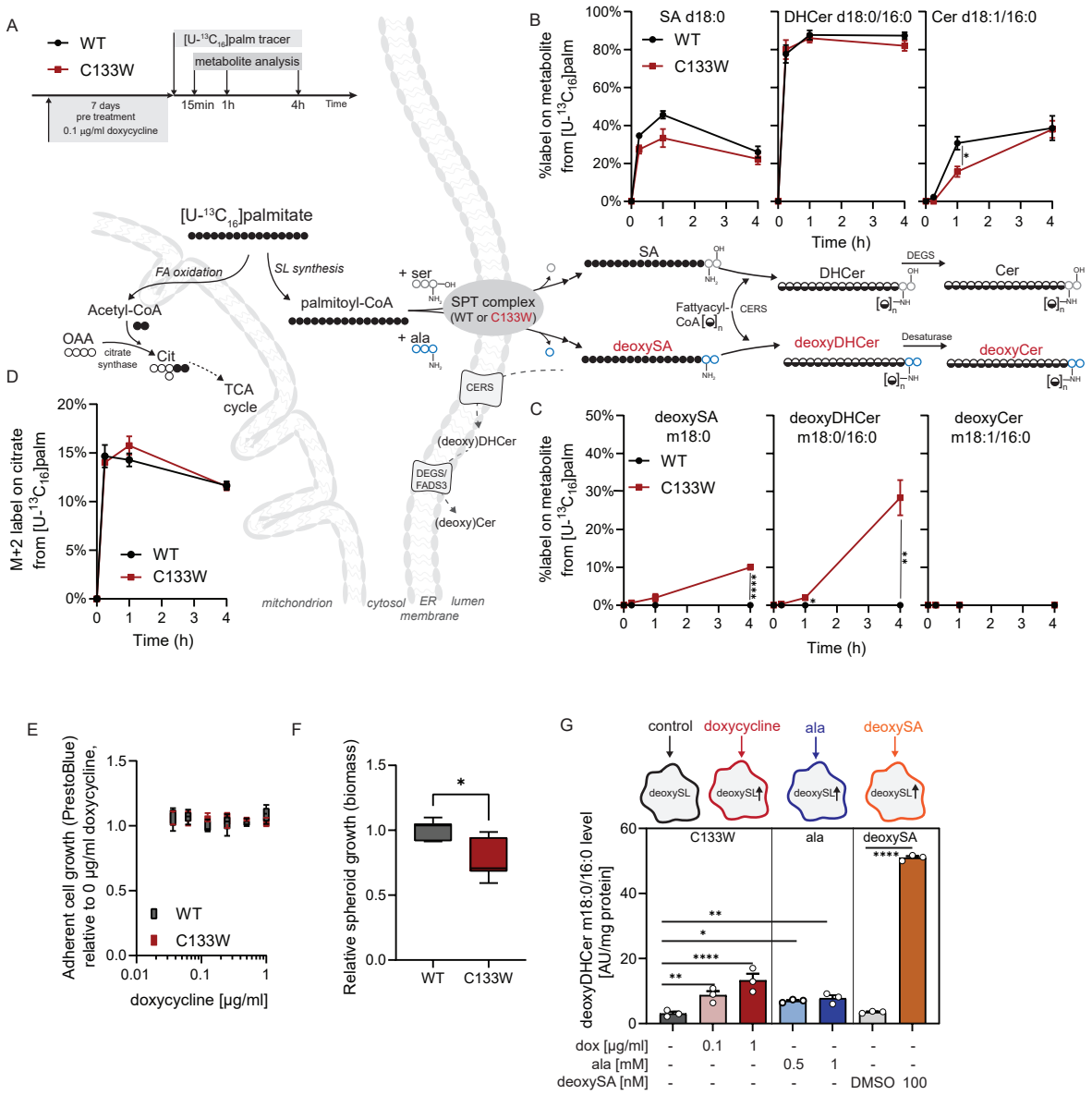

Figure 3: Impact of deoxySL synthesis on metabolic pathways

A. Schematic depicting trace into SL and deoxySL in engineered HCT116 cell lines cultured with 0.1 µg/ml doxycycline for 7 days prior tracing with [U-$^{13}C_{16}$]palmitate for 15min, 1h, and 4h.
B. Label on canonical SLs from ^{13}C palmitate tracer.
C. Label on non-canonical SLs from ^{13}C palmitate tracer.
D. Label on citrate from ^{13}C palmitate tracer.
E. Adherent cell growth of *SPT* expressing HCT116 cell lines cultured for 3 days with increasing doxycycline concentrations.
F. Spheroid growth in HCT116 *SPT* expressing cell lines with 0.1 µg/ml doxycycline.
G. DeoxyDHCer m18:0/16:0 levels in HCT116 *SPTLC1*^{C133W} expressing cells cultured for 3 days with alanine, doxycycline, or 100 nM deoxySA m18:0.

Data are presented as means ± s.e.m. with three cellular replicates (B, C, D, G) or box (25th to 75th percentile with median line) and whiskers (min. to max. values) (E, F). Student's *t*-test (B, D), nested *t*-test (F), or one-way ANOVA (G). Experiments in E, F, and G were repeated three times with similar results. Data in F depict average of 3 independent experiments with each 3 cellular replicates. *$P < 0.05$, ** $P < 0.01$, *** $P < 0.001$, **** $P < 0.0001$

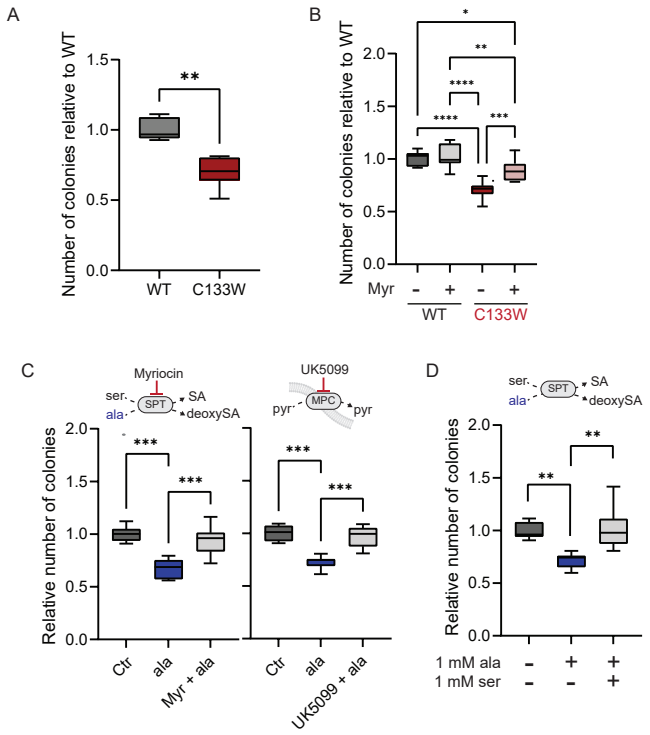

Figure 4: Alanine and deoxySL synthesis influence colony formation in soft agar

A. Colony formation in HCT116 wildtype (WT, grey) and mutant (C133W, red) *SPTLC1* expressing cells cultured for 7 days with 0.1 µg/ml doxycycline.
B. Colony formation in *SPTLC1* HCT116 cells with 10nM myriocin cultured for 7 days with 0.1 µg/ml doxycycline.
C. Colony formation in HCT116 cells with 1 mM alanine and 10 nM myriocin or 5 µM UK5099 cultured for 7 days with 0.1 µg/ml doxycycline.
D. Colony formation in HCT116 cells with 1 mM alanine and 1mM serine cultured for 7 days.

Data are presented as box (25th to 75th percentile with median line) and whiskers (min. to max. values) obtained from three independent experiments with each three cellular replicates. Nested *t*-test (A) or nested one-way ANOVA (B-D) with *$P < 0.05$, ** $P < 0.01$, *** $P < 0.001$, ****$P < 0.0001$.

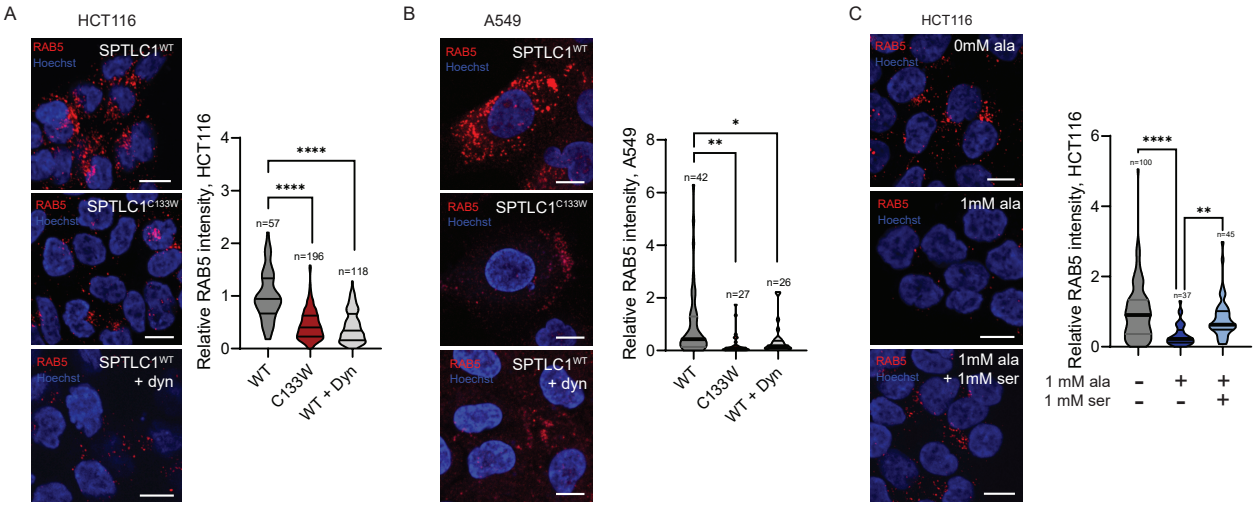

Figure 5: DeoxySLs compromise endocytosis.

A. RAB5 immunostaining with *SPTLC1*^{WT} and *SPTLC1*^{C133W} expressing HCT116 cultured for 4 days with 0.1 µg/ml doxycycline. Dynasore (dyn) was given with 20 µM for 3h.
B. RAB5 immunostaining with *SPTLC1*^{WT} and *SPTLC1*^{C133W} expressing A549 cultured for 4 days with 1 µg/ml doxycycline. Dynasore (dyn) was given with 20 µM for 3h.
C. RAB5 immunostaining with HCT116 cells cultured with 1mM alanine or 1mM serine.

Violin blots depict relative RAB5 intensity obtained from n= cell number. Data are representative of two independent experiments. White scale bar indicates 10 µm.

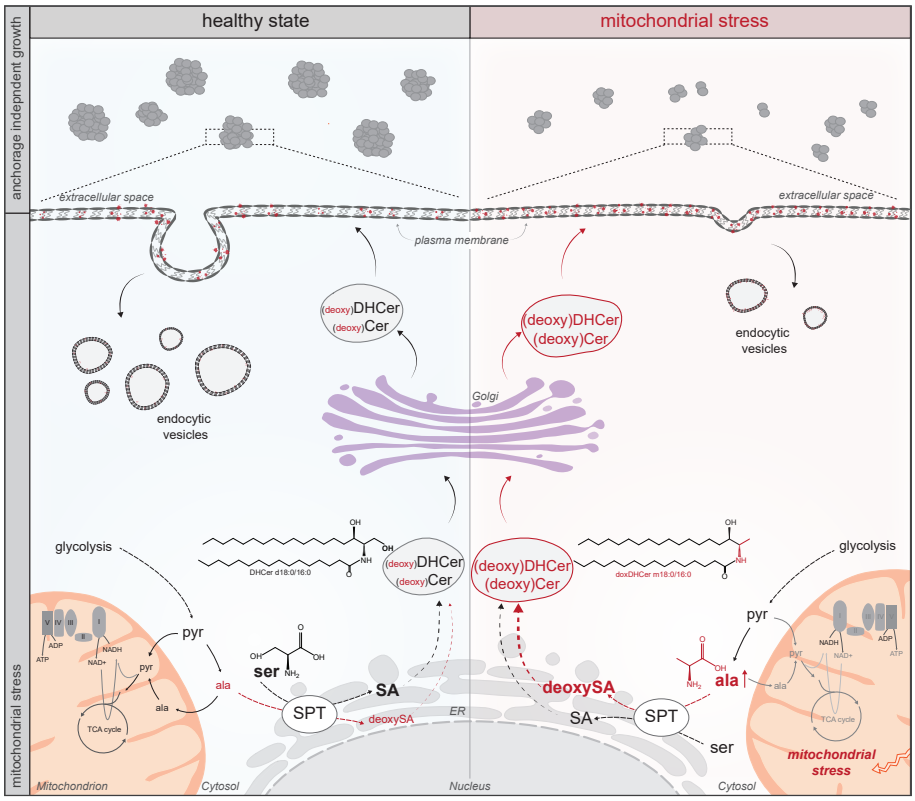

Figure 6: Schematic metabolic concept depicting metabolic impact of plasma membrane endocytosis through the lipidome compromising anchorage independent cell growth. SPT – serine palmitoyltransferase.